Layered Oxygen Deficient Double Perovskite as an Efficient and Stable Anode for Direct Hydrocarbon SOFCs

Sivaprakash Sengodan[1]†, Sihyuk Choi[1]†, Areum Jun[1], Tae Ho Shin[2], Young-Wan Ju[1], Hu Young Jeong[3], Jeeyoung Shin[4], John T.S Irvine[2]*, Guntae Kim[1]*

[1] *Department of Energy Engineering, Ulsan National Institute of Science and Technology (UNIST), Ulsan, 689–798, Korea*

[2] *School of Chemistry, University of St Andrews, St Andrews, Fife KY16 9ST, UK*

[3] *UNIST Central Research Facilities and School of Mechanical and Advanced Materials Engineering, UNIST, Ulsan, 689–798, Korea*

[4] *Department of Mechanical Engineering, Dong-Eui University, Busan 614-714, Korea*

† These authors contributed equally to this work.

Different layered perovskite related oxides are known to exhibit important electronic, magnetic and electrochemical properties. Due to their excellent mixed-ionic and electronic conductivity and fast oxygen kinetics, cation layered double perovskite oxides such as $PrBaCo_2O_5$ in particular have exhibited excellent properties as solid oxide fuel cell oxygen electrodes[1]. Here we show for the first time that related layered materials can be used as high performance fuel electrodes. Good redox stability with tolerance to coking and sulfur contamination from hydrocarbon fuels is demonstrated for the layered perovskite anode, $PrBaMn_2O_{5+\delta}$ (PBMO). The PBMO anode is fabricated by in-situ annealing of $Pr_{0.5}Ba_{0.5}MnO_{3-\delta}$ in fuel conditions and actual fuel cell operation is demonstrated. At 800 ^oC, layered PBMO shows high electrical conductivity of 8.16 S cm^{-1} in 5% H_2 and

demonstrates peak power densities of 1.7 and 1.3 W cm^{-2} at 850 ^{o}C using humidified hydrogen and propane fuels, respectively.

Solid oxide fuel cells are electrochemical energy conversion devices that directly convert the chemical energy in fuel to electricity with very high energy efficiency and excellent fuel flexibility[1-3]. The conventional Ni/electrolyte composite anode, Ni cermet, has high catalytic activity towards fuel oxidation but it is deactivated during operation because of its sensitivity to carbon buildup from incomplete oxidation of hydrocarbons and sulfur poisoning by contaminants commonly encountered in readily available fuels[4]. To overcome these problems, various alternative anode materials and/or material combinations prepared via incorporation of other materials have been studied as potential SOFC anodes. Gorte *et al*. reported Cu-CeO_2-yttria-stabilised zirconia (YSZ) composite anodes operated on a range of dry hydrocarbons with good carbon and sulfur tolerance[5]. Cu particles, however, tend to coarsen over time due to their relatively low melting point (1085 ^{o}C), causing poor electronic conduction[6], they also have poor catalytic activity for direct hydrocarbon oxidation[7], limiting the power output. To retain the high-performance of Ni based anodes in hydrocarbon fuels, a Ru-CeO_2 catalyst layer was later applied on a conventional Ni-YSZ anode to prevent carbon coking due to the internal reforming of *iso*-octane[8]. However, drawbacks such as a large amount of CO_2 and O_2 being co-fed with *iso*-octane, difficulties in current collection, and the high cost of Ru may limit practical application of this catalyst[8,9]. Recently, Liu *et al*, adopted a different strategy to achieve high tolerance to coking and sulfur poisoning. They replaced the oxide ion conductor in the conventional in Ni-YSZ anode with a mixed ion conductor (it conducts both H^+ and O^{2-}), e.g. co-doped Y and Yb at

$BaZrO_3$-$BaCeO_3$[10]. The $BaZrO_3$-$BaCeO_3$ anode, however, requires high sintering temperature (> 1700 ^oC) during cell fabrication due to its poor sinterability. As a result, it is incompatible with YSZ and it also shows poor chemical stability with CO_2 and H_2O under operational conditions[11].

Alternatively, mixed oxide-ion electron conductors (MIECs) have been developed as ceramic anode materials. Examples include $La_{0.8}Sr_{0.2}Sc_xMn_{1-x}O_{3-\delta}$[12], $La_{0.33}Sr_{0.67}Ti_xMn_{1-x}O_{3-\delta}$[13], $Y_{0.08}Sr_{0.92}Ti_{1-x}Fe_xO_{3-\delta}$[14], $La_{0.75}Sr_{0.25}Cr_{0.5}Mn_{0.5}O_3$ (LSCM)[15], Sr_2MgMoO_6 (SMMO)[16], $Pr_{0.8}Sr_{1.2}(Co,Fe)_{0.8}Nb_{0.2}O_4$ (K-PSCFN)[17], and $Ce_{0.6}Mn_{0.3}Fe_{0.1}O_2$-$La_{0.6}Sr_{0.4}Fe_{0.9}Mn_{0.1}O_3$ (CMF-LSFM)[18]. These anodes are stable in anodic operating conditions and demonstrate improved coking tolerance and sulfur poisoning under various fuel conditions. However, the catalytic activity, electrical conductivity, and power density of these MIEC anodes are much lower than those of the conventional Ni-YSZ anode. For example, without a Pd oxidation catalyst, the LSCM anode backbone cannot perform reliably in H_2 and CH_4 below 900 ^oC[19]. Meanwhile, it has been suggested that the electrochemical performance of the SMMO anode is sensitive to current collectors[16]. Recently, a K_2NiF_4 type K-PSCFN anode with Co-Fe alloy as an oxidation catalyst was reported. The cell performance dropped significantly after oxidation back to a perovskite-type structure, although it provided coking resistance and sulfur tolerance[17]. The CMF-LSFM composite oxide was also reported to be a good ceramic anode with improved power density in propane, e.g. ~1 W cm^{-2} at 800 ^oC, but the power densities in H_2 and CH_4 are unacceptably low[18].

In this work, in order to obtain high electrochemical performance along with high tolerance to carbon coking and H_2S poisoning, we present a novel redox stable MIEC anode

consisting of an A-site layered double perovskite structure, $PrBaMn_2O_{5+\delta}$ (PBMO), for operation on hydrocarbon fuel. We selected this double perovskite system based on the following factors:

a) Degree of A-site ordering: layered PBMO is thermally and chemically stable under fuel electrode conditions[20,21].

b) Higher electrical conductivity and oxygen kinetics: The layered PBMO perovskite structure supports mixed valent transition metal cations ($Mn^{4+}/Mn^{3+}/Mn^{2+}$), which could provide high electrical conductivity and maintain a large oxygen vacancy content, contributing to fast oxygen ion diffusion[22].

c) Good catalytic activity toward both hydrogen and hydrocarbon oxidation: Perovskite oxides of first row transition metals containing Mn, Co, and Fe rich perovskite provide high activity in hydrocarbon oxidation[23,24].

A-site layered PBMO oxide is obtained by annealing $Pr_{0.5}Ba_{0.5}MnO_{3-\delta}$ oxide (cubic/hexagonal) in H_2 at 800 ^oC (Supplementary Fig. 1). A-site layered compounds are best synthesized by a two-step sintering process. $Pr_{0.5}Ba_{0.5}MnO_{3-\delta}$ was synthesized in air at 950 ^oC via the Pechini synthesis method and the air prepared sample was treated in a reducing atmosphere to step down the oxygen from the "O_3" to "O_5" phase[20].

$$Pr_{0.5}Ba_{0.5}MnO_3 \xrightarrow[800\,^{\circ}C,\,H_2]{} PrBaMn_2O_5 \quad (1)$$

where the "O_5" phase is characterized by layered alternate stacking of Pr^{3+} ions and Ba^{2+} O^{2-} layers along the c-axis. Subsequently, the A-site in the unit cell of the "O_5" phase is doubled[21] and can be characterized as A-site layered perovskite ("O_5"). The phase change is

associated with this reduction confirmed by DTA-TGA in Fig. 1, which clearly shows the presence of a sharp exothermic peak (*) upon heating at 400 ^{o}C. The phase change of $Pr_{0.5}Ba_{0.5}MnO_{3-\delta}$ to layered PBMO is also observed by *in*-situ XRD in reducing conditions (Supplementary Fig.2).

Although Pr^{3+} and Ba^{2+} are close to isoelectronic, the Pr ion is significantly smaller than Ba in similar coordination, PBMO thus adopts a layered crystal structure, wherein an MnO_2 square sublattice is sandwiched between two rock salt layers, PrO_x and BaO layers, along the c-axis ([BaO]-[MnO_2]-[PrO_x]-[MnO_2]-[BaO]. A site layered PBMO has a remarkable structural feature: Under reducing conditions, oxygen atoms in the PrO_x plane can be partially or entirely removed, creating many oxygen vacant sites in the crystal sites.

Figure 2 shows transmission electron microscopy (TEM) images of air-prepared $Pr_{0.5}Ba_{0.5}MnO_{3-\delta}$ and layered PBMO samples. The air-prepared powder sample shows a smooth surface morphology with a high crystal quality, as seen in bright-field (BF) TEM and high-resolution (HR) TEM images (Fig. 2a,b). However, it is notable that the morphology of particles is dramatically changed after annealing in H_2 at 800 ^{o}C. Figures 2d,e show that layered PBMO particles have a rough surface morphology with many facets and defects, as represented by red arrows in Fig. 2e. This could result in the increase of a surface area (e.g., 2.42 and 5.32 m^2 g^{-1} for $Pr_{0.5}Ba_{0.5}MnO_{3-\delta}$ and layered PBMO, respectively) and electrochemically active site. Furthermore, the A-site ordering was observed by showing a weak additional spot in fast-Fourier transformed (FFT) pattern, which is indexed with (001) of tetragonal superlattice. It can be also confirmed in high-angle annular dark field (HAADF) scanning TEM (STEM) image Fig. 2f,

indicating a periodic contrast change due to A-site ordering of PrO and BaO layers, compared to even contrast in Fig. 2c.

The novel PBMO layered perovskite structure retains high electrical conductivity in both air and hydrogen atmospheres. Figure 3a shows the electrical conductivity of layered PBMO as a function of temperature in air and wet 5% H_2. An ideal SOFC anode must have sufficiently high electrical conductivity in order to provide efficient electron transfer paths. In this regard, for SMMO and LSCM electrical conductivities of 4.21 and 0.96 S cm^{-1} at 800 ^oC in 5% H_2, respectively, were obtained[15,16]. Meanwhile, the electrical conductivity of layered PBMO is as high as 8.16 S cm^{-1} in 5 % H_2 and 91.5 S cm^{-1} in air. Under reducing conditions, oxygen vacancies are formed and the predominant defect species in layered PBMO are mobile electronic holes, $h^{\bullet} = Mn_{Mn}^{\bullet}$. The interaction between the oxygen and the defects in the layered PBMO can be expressed as follows,

$$2Mn_{Mn}^{\times} + \frac{1}{2}O_2 + V_O^{\bullet\bullet} \leftrightarrows O_O^{\times} + 2Mn_{Mn}^{\bullet} \qquad (2)$$

The concentration of oxygen vacancies will increase under a reducing atmosphere according to equation (2). This may lead to enhanced oxide-ionic conductivity and oxygen ion transfer sites between the anode and the electrolyte. Figure 3b shows the relation between oxygen non-stoichiometry and $p(O_2)$ for layered PBMO oxides at 650-750 ^oC. The initial oxygen content of the layered PBMO was determined by iodometric titration and a TGA analysis (Supplementary Fig. 3). In the high $p(O_2)$ region, the electrical charge was mainly balanced by the formation of Mn^{4+} ions (although some Pr^{4+} may be present), while on reduction electroneutrality was maintained by the formation of oxygen vacancies followed by the reduction of Mn^{4+} to Mn^{3+} and

Mn^{3+} to Mn^{2+} ion in the low $p(O_2)$ region. From Fig. 3b, the amount of oxygen vacancies in the layered PBMO oxide after reduction is roughly δ = 0.74 or 2.49 wt %, indicating the layered phase has stoichiometry $PrBaMn_2O_{5.74}$ which is a much higher level of vacancies than that of other ceramic anodes, such as LSCM and SMMO[25,26]. Dilatometry experiments confirm that this process is reversible with the reduction occurring between 350 and 600 ^oC and the reoxidation at as low a temperature as 200 ^oC (Supplementary Fig. 4). The associated chemical expansion was 0.7 %. On heating in air, a similar reduction towards this layered double perovskite at 1050 ^oC, although this is not complete by 1450 ^oC (Supplementary Fig. 5).

To characterize the performance of the novel layered PBMO anode material in a practical fuel cell, we used electrolyte-supported cells based on a ~300 μm thick $La_{0.9}Sr_{0.1}Ga_{0.8}Mg_{0.2}O_{3-\delta}$ (LSGM) electrolyte. A-site layered PBMO was obtained by (in-situ phase change at SOFC setup) annealing $Pr_{0.5}Ba_{0.5}MnO_{3-\delta}$ oxide in H_2 at 800 ^oC. Instead of Pt, Ag paste was applied as the current collector to avoid possible extraneous catalytic effects on fuel oxidation. The fuel cell performance of a single cell with the configuration of PBMO/$La_{0.4}Ce_{0.6}O_{2-\delta}$ (LDC)/LSGM/$NdBa_{0.5}Sr_{0.5}Co_{1.5}Fe_{0.5}O_{5+\delta}$-$Ce_{0.9}Gd_{0.1}O_{2-\delta}$ (NBSCF50-GDC) was tested using various humidified (3% H_2O) fuels (H_2, C_3H_8 and CH_4) and ambient air as an oxidant. The maximum power density of the layered PBMO cell without any catalysts in H_2 was 0.57 W cm^{-2} at 850 ^oC (Supplementary Fig. 6)**.** In case of adding additional PBMO as a catalyst by infiltration into the porous layered PBMO cell, the maximum power densities (Supplementary Fig. 7) were 1.57, 1.07, and 0.76 W cm^{-2} at 850, 800, and 750 ^oC in H_2, respectively, and very stable performance under a constant current load of 1.0 A cm^{-2} at 700 ^oC was shown in Supplementary Fig. 8. Moreover, with humidified C_3H_8 and CH_4 as the fuel, the maximum

power densities and impedance spectra of the layered PBMO cell with the PBMO catalyst at 850 ^{o}C are presented in Fig. 4a and Supplementary Figs 9-11. As there is no great difference in microstructure after reduction between without and with PBMO infiltration (Supplementary Fig. 12), it seems that the infiltrated PBMO exhibits high electrocatalytic activity for H_2 and propane fuels and moderate activity for methane. At fuel cell operation temperatures, propane pyrolysis would be anticipated[27] yielding hydrogen, various short chain hydrocarbons and coke or tar, in accord with the initial C:H:O ratios of 27:23:0.3, which is within the thermodynamic range for coking at these temperatures[28]. This is indeed supported by our supplementary studies showing large concentration of hydrogen, methane and ethane in the gas stream (Supplementary Fig. 13). Exit gases from the fuel cell test show similar gas products; however, there is also significant concentration of carbon oxides confirming direct and/or indirect oxidation of the hydrocarbon fuels by produced oxygen (Supplementary Fig. 14 and Supplementary Table 1). The observed absence of coking especially under the presented 500 h studies shows improved catalytic effects for higher hydrocarbon oxidation, which may originate from the Mn on the B-site in perovskite oxides[15,24], although Pr is also known to facilitate electrode reactions due to its mixed valence capability.

We also evaluated the performance of a layered PBMO cell with a 15 wt % Co-Fe catalyst under humidified (3% H_2O) H_2, C_3H_8 and CH_4 (Supplementary Figs 15-18). The maximum power densities of layered PBMO with the Co-Fe catalyst reached 1.77, 1.32, and 0.57 W cm^{-2} at 850 ^{o}C, in humidified H_2, C_3H_8, and CH_4, respectively, as shown in Fig. 4b. The maximum power density of layered PBMO with the Co-Fe catalyst is slightly improved in comparison with use of only the PBMO catalyst in H_2. With both C_3H_8 and CH_4 as a fuel,

however, the performance of layered PBMO with the Co-Fe catalyst is considerably enhanced compared to the case of the PBMO catalyst.

We also systematically investigated the layered PBMO anode in various ppm H_2S-contaminated H_2 (Supplementary Figs 19 and 20). The power densities of layered PBMO with PBMO and Co-Fe catalysts respectively were 1.42 and 1.64 W cm^{-2} at 850 ^oC in 50 ppm H_2S contaminated H_2 (Fig. 4a,b). To assess the sulfur tolerance of PBMO with the Co-Fe catalyst, a constant current of 1.0 A cm^{-2} was applied at 700 ^oC, while the fuel was changed from H_2 to 30 ppm H_2S/H_2, as shown in Fig. 4c. After stabilizing the cells for 50 h under pure H_2, the atmosphere was changed to contain 30 ppm H_2S. The cell voltage of layered PBMO with the Co-Fe catalyst shows no observable degradation, indicating that the layered PBMO anode has excellent sulfur tolerance. The coking resistance of the layered PBMO anode with the Co-Fe catalyst was demonstrated in humidified propane (Fig. 4d). Normally, carbon can easily build up on a conventional Ni-based anode when directly operated on such fuel. However, no degradation was observed from carbon coking under a constant current load of 0.2 A cm^{-2} at 700 ^oC in C_3H_8 for more than 500 h.

In summary, a novel A-site layered double perovskite- manganese oxide demonstrates superior SOFC anode performance and stability in various fuels. Layered PBMO anodes exhibit high electrical conductivity, excellent redox and coking tolerance and sulfur tolerance. Furthermore, on the basis of its remarkable stability in reducing conditions, layered PBMO is an attractive ceramic anode material for SOFCs.

Methods

The $Pr_{0.5}Ba_{0.5}MnO_{3-\delta}$ was prepared by the Pechini method. A-site layered PBMO anode is obtained by annealing $Pr_{0.5}Ba_{0.5}MnO_{3-\delta}$ oxide in H_2 at 800 ^{o}C. The initial structural characterization of the PBMO oxide was performed by X-ray diffractometry by Rigaku diffractometer (Cu Kα radiation, 40 kV, 30 mA) and *in*-situ X-ray diffraction (PANalytical Empyrean, Mo Kα radiation). Transmission electron microscopy (TEM) was used to characterize the detailed microscopic features and cation ordering in the structure.

Electrical conductivity was measured as a function of temperature using the standard four-probe technique with a BioLogic Potentiostat. Thermogravimetric analyses (TGA) were performed at 100 ^{o}C to 800 ^{o}C with a heating/cooling rate of 2 ^{o}C min^{-1} in air and 5% H_2 to characterize the thermo-physical properties. The oxygen non-stoichiometry at elevated temperature was studied through Coulometric titration (CT) by measuring the oxygen partial pressure of PBMO oxides as a function of temperature, as reported elsewhere[29].

For fuel cell performance, a configuration of PBMO/LDC/LSGM/NBSCF50-GDC was fabricated based on 300 μm LSGM electrolyte-supported cells (Supplementary Fig. 21). LDC layer was used as the buffer layer between the anode and the electrolyte to prevent inter-diffusion of ionic species between PBMO and LSGM. The anode and cathode slurries were applied on the LSGM pellet by screen printing method, and then fired at 950 ^{o}C in air for 4 h. 15 wt% of PBMO or $Co_{0.5}Fe_{0.5}$ (Co-Fe) catalyst solution was infiltrated onto the anode side and heated in air at 450 ^{o}C. *V–i* polarization curves were measured using a BioLogic Potentiostat in the temperature range of 700-850 ^{o}C.

References

1. Choi, S., Yoo, S., Kim, J., Park, S., Jun, A., Sengodan, S., Kim, J., Shin, J., Jeong, H. Y., Choi, Y., Kim, G., Liu, M. Highly efficient and robust cathode materials for low-temperature solid oxide fuel cells: $PrBa_{0.5}Sr_{0.5}Co_{2-x}Fe_xO_{5+\delta}$. *Sci Rep*. **3,** 2426 (2013).
2. Wang, W., Su, C., Wu, Y., Ran, R., Shao, Z. Progress in Solid Oxide Fuel Cells with Nickel-Based Anodes Operating on Methane and Related Fuels. *Chemical Reviews* **113**, 8104-8151(2013).
3. Atkinson, A., Barnett, S., Gorte, R. J., Irvine, J. T. S., McEvoy, A. J., Mogensen, M., Singhal, S. C., Vohs, J. Advanced anodes for high-temperature fuel cells. *Nat. Mater.* ***3,***17-27 (2004).
4. Liu, M., Lynch, M. E., Blinn, K., Alamgir, F. M., Choi, Y. Rational SOFC material design: new advances and tools. *Mater. Today.* **14**, 534-546 (2011)**.**
5. Park, S., Vohs, J. M., Gorte, R. J. Direct oxidation of hydrocarbons in a solid-oxide fuel cell. *Nature* **404**, 265-267 (2000**)**.
6. Cheng, Z., Wang, J.-H., Choi, Y., Yang, L., Lin, M. C., Liu, M. From Ni-YSZ to sulfur-tolerant anode materials for SOFCs: electrochemical behavior, in situ characterization, modeling, and future perspectives. *Energy Environ.Sci.* **4,** 4380-4409 (2011).
7. He, H., Gorte, R. J., Vohs, J. M. Highly Sulfur Tolerant Cu-Ceria Anodes for SOFCs. *Electrochem. Solid State Lett.* **8,** A279-A280 (2005).
8. Zhan, Z., Barnett, S. A. An Octane-Fueled Solid Oxide Fuel Cell. *Science* **308**, 844-847 (2005).

9. Liu, M., Choi, Y.; Yang, L., Blinn, K., Qin, W., Liu, P., Liu, M. Direct octane fuel cells: A promising power for transportation. *Nano Energy* **1**, 448-455 (2012).

10. Yang, L., Wang, S., Blinn, K., Liu, M., Liu, Z., Cheng, Z., Liu, M. Enhanced Sulfur and Coking Tolerance of a Mixed Ion Conductor for SOFCs: $BaZr_{0.1}Ce_{0.7}Y_{0.2-x}Yb_xO_{3-\delta}$. *Science* **326**, 126-129 (2009).

11. Ryu, K. H., Haile, S. M. Chemical stability and proton conductivity of doped $BaCeO_3$–$BaZrO_3$ solid solutions. *Solid State Ionics* **125**, 355-367 (1999).

12. Sengodan.S, Yeo. H. J, Shin J. Y, Kim. G. Assessment of Perovskite-type $La_{0.8}Sr_{0.2}Sc_xMn_{1-x}O_{3-\delta}$ Oxides as an Anode for Intermediate Temperature Solid Oxide Fuel Cells using Hydrocarbon. *J. Power sources*, **196**, 3083-3088 (2011).

13. Corre. G, Kim. G, Cassidy. M, Vohs. J. M, Gorte. R. J, Irvine. J. T. S. Activation and Ripening of Impregnated Manganese Containing Perovskite SOFC Electrodes under Redox Cycling. *Chem. Mater*, **21**, 1077-1084 (2009).

14. Sengodan. S, Yoon. J. S, Yoon. M. Y, Hwang. H. J, Shin J. Y, Kim. G. Electrochemical performance of YST infiltrated and Fe doped YST infiltrated YSZ anodes for IT-SOFC. *ECS Electrochem. Lett*. **2**, F45-F49 (2013).

15. Tao, S., Irvine, J. T. S. A redox-stable efficient anode for solid-oxide fuel cells. *Nat Mater.* **2**, 320-323 (2003).

16. Huang, Y.-H., Dass, R. I., Xing, Z.-L., Goodenough, J. B. Double Perovskites as Anode Materials for Solid-Oxide Fuel Cells. *Science* **312**, 254-257 (2006).

17. Yang, C., Yang, Z., Jin, C., Xiao, G., Chen, F., Han, M. Sulfur-Tolerant Redox-Reversible Anode Material for Direct Hydrocarbon Solid Oxide Fuel Cells. *Adv. Mater.* **24**, 1439-1443 (2012).

18. Shin, T. H., Ida, S., Ishihara, T. Doped CeO_2–$LaFeO_3$ Composite Oxide as an Active Anode for Direct Hydrocarbon-Type Solid Oxide Fuel Cells. *J. Am. Chem. Soc.* **48**, 19399-19407 (2011).

19. Kim, G., Corre, G., Irvine, J. T. S., Vohs, J. M., Gorte, R. J. Engineering Composite Oxide SOFC Anodes for Efficient Oxidation of Methane. *Electrochem. Solid State Lett.* **11**, B16-B19 (2008).

20. Trukhanov, S.V., Lobanovski, L.S., Bushinsky, M.V., Fedotova, V.V., Troyanchuk, I.O., Trukhanov, A.V., Ryzhov, V. A., Szymczak, H., Szymczak, R., Baran, M. Study of A-site ordered $PrBaMn_2O_{6-\delta}$ manganite properties depending on the treatment conditions. *J Phys. Condens. Matter.* **17**, 6495 (2005).

21. Trukhanov, S.V., Trukhanov, A.V., Szymczak, H., Szymczak, R., Baran, M. Thermal stability of A-site ordered $PrBaMn_2O_6$ manganites. *J Phys. Chem. Solids.* **67**, 675-81(2006).

22. Taskin, A.A., Lavrov, A.N., Ando, Y. Fast oxygen diffusion in A-site ordered perovskites. *Prog. Solid State Chem.* **35**, 481-490 (2007).

23. Danilovic, N., Vincent, A., Luo, J-L., Chuang, K.T., Hui, R., Sanger, A.R. Correlation of Fuel Cell Anode Electrocatalytic and ex situ Catalytic Activity of Perovskites $La_{0.75}Sr_{0.25}Cr_{0.5}X_{0.5}O_{3-\delta}$ (X = Ti, Mn, Fe, Co). *Chem. Mater.* **22**, 957-965 (2009).

24. Motohashi, T., Ueda, T., Masubuchi, Y., Takiguchi, M., Setoyama, T., Oshima, K., Kikkawa, S. Remarkable Oxygen Intake/Release Capability of $BaYMn_2O_{5+\delta}$: Applications to Oxygen Storage Technologies. *Chem. Mater.* **22,** 3192-3196 (2010).

25. Oishi, M., Yashiro, K., Sato, K., Mizusaki, J., Kawada, T. Oxygen nonstoichiometry and defect structure analysis of B-site mixed perovskite-type oxide (La, Sr)(Cr, M)$O_{3-\delta}$ (M=Ti, Mn and Fe). *J. Solid State Chem.* **181**, 177-184 (2008).

26. Marrero-López, D., Peña-Martínez, J., Ruiz-Morales, J.C., Gabás, M., Núñez, P., Aranda, M.A.G., Ramos-Barrado, J. R. Redox behaviour, chemical compatibility and electrochemical performance of $Sr_2MgMoO_{6-\delta}$ as SOFC anode. *Solid State Ionics* **180**, 1672-1682 (2010).

27. Volkan, A. G., April, G. C. Survey of propane pyrolysis literature. *Ind. Eng. Chem. Process Des. Dev.***16(4)** 429-436 (1977).

28. Sasaki, K., Teraoka, Y. Equilibria in Fuel Cell Gases I. Equilibrium Compositions and Reforming Conditions. *J. Electrochem. Soc.* **150 (7)** A878-A884 (2003).

29. Sengodan, S., Ahn, S., Shin, J., Kim, G. Oxidation–reduction behavior of $La_{0.8}Sr_{0.2}Sc_yMn_{1-y}O_{3\pm\delta}$ (y=0.2, 0.3, 0.4): Defect structure, thermodynamic and electrical properties. *Solid State Ionics* **228**, 25-31 (2012).

Acknowledgements

This research was supported by the New & Renewable Energy of the Korea Institute of Energy Technology Evaluation and Planning (KETEP) (20113020030060) grant by the Korea government Ministry of Trade, Industry and Energy, Mid-career Researcher Program (2013R1A2A2A04015706) through the National Research Foundation of Korea, funded by the Ministry of Science, ICT and Future Planning and the Basic Science Research Program (2013R1A2A2A01007170 and 2010-0021214) through the National Research Foundation of Korea, funded by Ministry of Education. We thank The Royal Society for a Wolfson Merit Award (JI) and EPSRC for a research grant (EP/I022570/1).

Author contributions

S.S., S.C., and A.J. contributed to fabricate samples and conducted data analysis of all kinds of electrochemical experiments, SEM, C.T, XRD, and GC. Y.W.J. fabricated samples and discussed electrochemical data. T.H.S carried out the HTXRD and dilatometer. H.Y.J. collected and analyzed the TEM data. J.S, J.T.S.I., and G.K. conceived and designed the project. All authors contributed to writing the paper.

Competing financial interests

The authors declare no competing financial interests.

Figures

Figure 1 | Principle of the approach to prepare A-site layered perovskite $PrBaMn_2O_{5+\delta}$

Phase change of $Pr_{0.5}Ba_{0.5}MnO_3$ to layered $PrBaMn_2O_{5+\delta}$ occurs under reducing atmosphere. The DTA curve shows the presence of sharp exothermic peak (*) upon heating at 400 ^oC. A-site layered $PrBaMn_2O_{5+\delta}$ shows that MnO_2 square sublattice is sandwiched between two rock salt layers, PrO and BaO layers, along the c axis.

Figure 2 | Transmission electron microscopy (TEM) analysis a, Bright field (BF) TEM. **b,** High-resolution (HR) TEM image and corresponding fast-Fourier transformed (FFT) pattern. **c,** High angle annular dark field (HAADF) scanning TEM (STEM) image of $Pr_{0.5}Ba_{0.5}MnO_3$ and its atomic arrangement viewed at [100] direction. **d**, BF-TEM image. **e**, HR-TEM image and corresponding FFT pattern, **f**, HAADF STEM image of A-site layered $PrBaMn_2O_{5+\delta}$ and its atomic arrangement aligned along [100] direction.

Figure 3 | Electrical and redox properties of layered $PrBaMn_2O_{5+\delta}$ a, Temperature dependence of total conductivity of layered PBMO in air and humidified 5% H_2. **b,** Oxygen non-stoichiometry of layered PBMO as a function of $p(O_2)$ at 650, 700, and 750 ^oC. Insets are schematics of layered $PrBaMn_2O_5$ and $PrBaMn_2O_{5+\delta}$ at low and high pO_2 region, respectively.

Figure 4 | Electrochemical properties of layered $PrBaMn_2O_{5+\delta}$ anode with $PrBaMn_2O_{5+\delta}$ and Co-Fe catalyst in fuel cells *I-V* curves and the corresponding power densities of layered PBMO with **a,** layered PBMO catalyst and **b,** Co-Fe catalyst using a humidified (3% H_2O) various fuel and ambient air as the oxidant at 850 ^oC. **c,** Short term stability for a layered PBMO with Co-Fe catalyst under a constant current load of 1.0 A cm^{-2} at 700 ^oC in H_2 and H_2-30ppm

H_2S. **d,** Long term stability test of layered PBMO with Co-Fe catalyst under a constant current load of 0.2 A cm^{-2} at 700 ^oC in C_3H_8.

$Pr_{0.5}Ba_{0.5}MnO_3$

Pr
Ba
Mn
O

*

Phase change
under reducing
atmosphere

Layered
$PrBaMn_2O_{5+\delta}$

Weight change (%)

102
101
100
99
98
97
96
95
94

Heat flow (ΔT)

0
200
400
600
800

Temperature (°C)

a

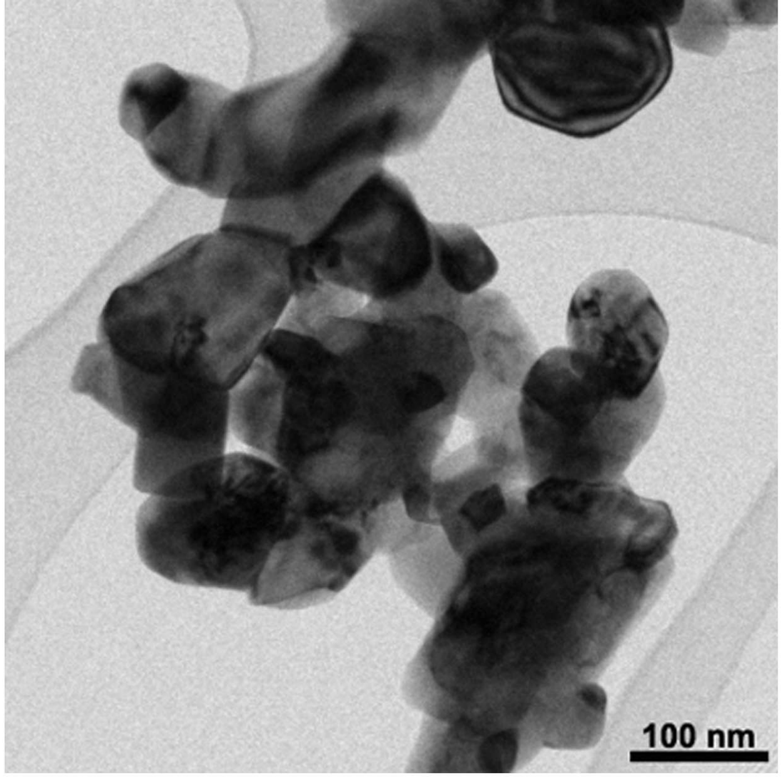
100 nm

b

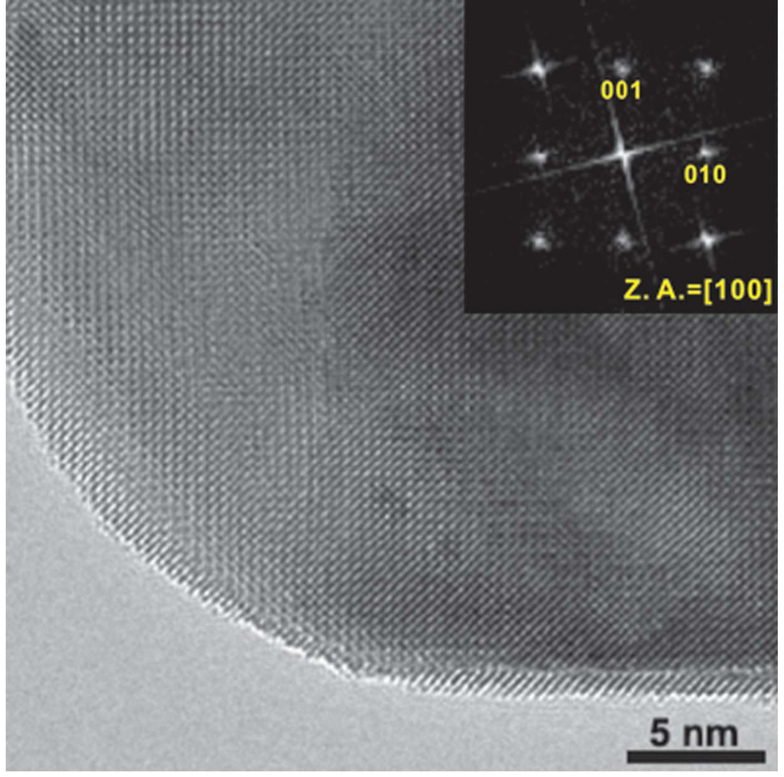
001
010
Z. A.=[100]
5 nm

c

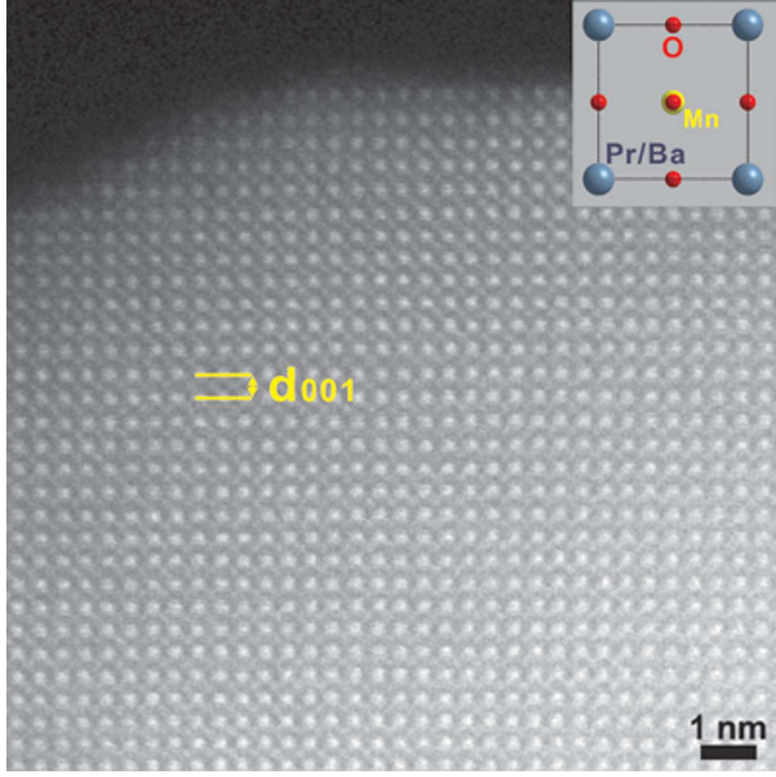
O
Mn
Pr/Ba
d001
1 nm

d

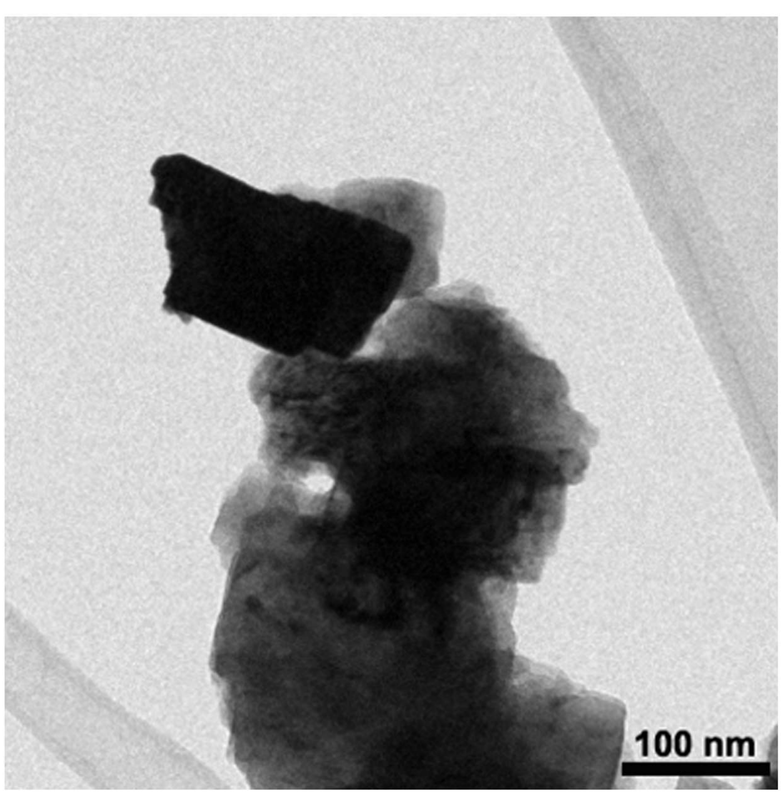
100 nm

e

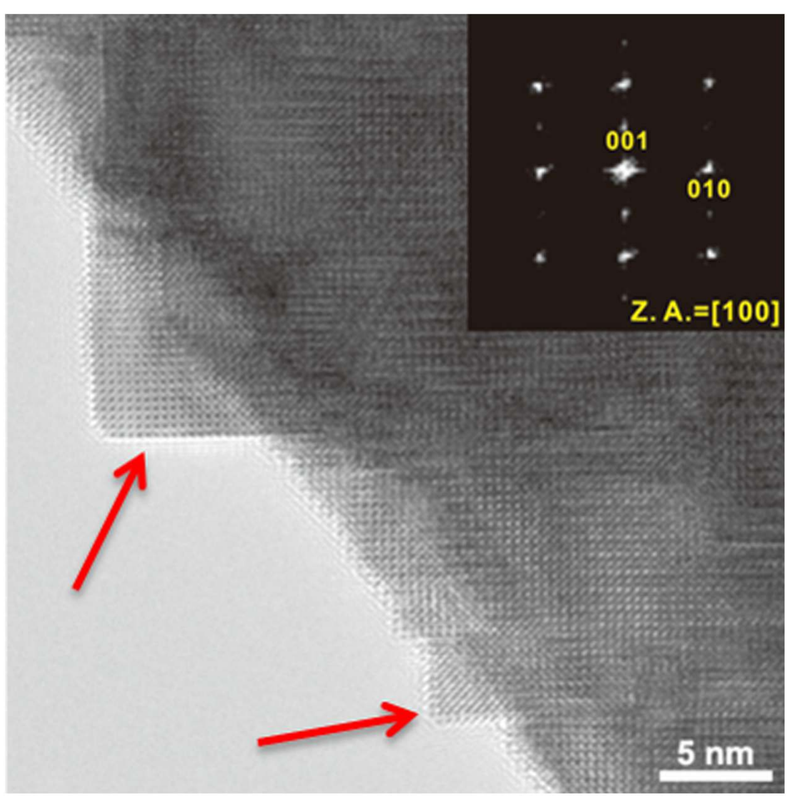
001
010
Z. A.=[100]
5 nm

f

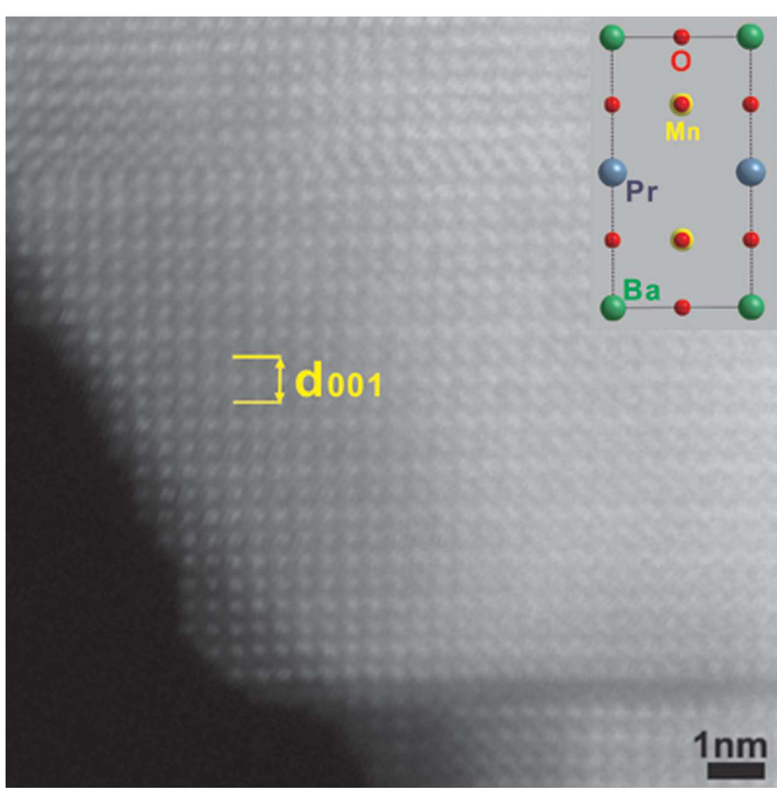
O
Mn
Pr
Ba
d001
1nm

a

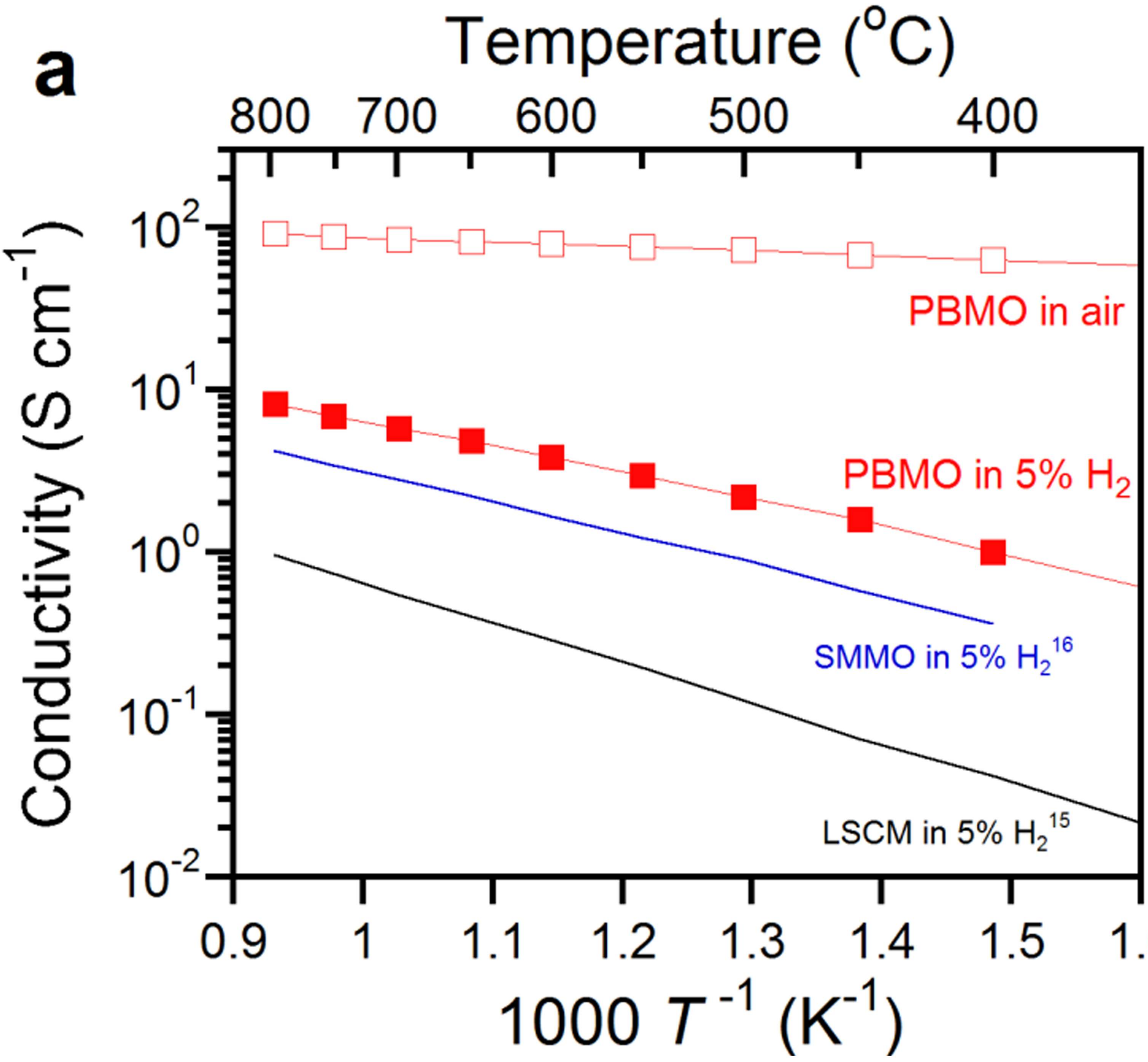
Temperature (°C)
800
700
600
500
400
Conductivity (S cm-1)
10^2
10^1
10^0
10^-1
10^-2
PBMO in air
PBMO in 5% H2
SMMO in 5% H2 16
LSCM in 5% H2 15
0.9
1
1.1
1.2
1.3
1.4
1.5
1.6
1000 T -1 (K-1)

b

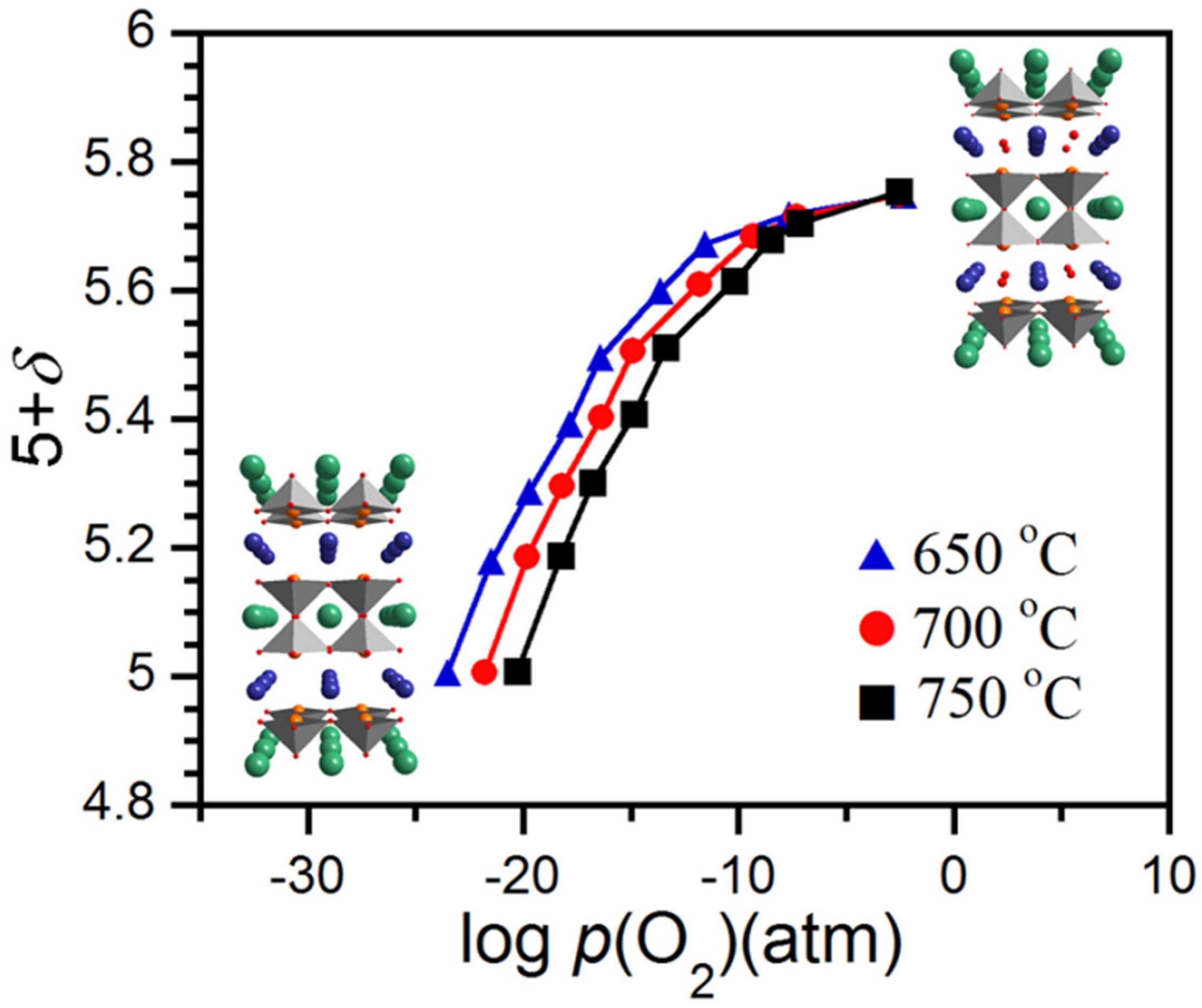
6
5.8
5.6
5.4
5.2
5
4.8
5+δ
650 °C
700 °C
750 °C
-30
-20
-10
0
10
log p(O2)(atm)

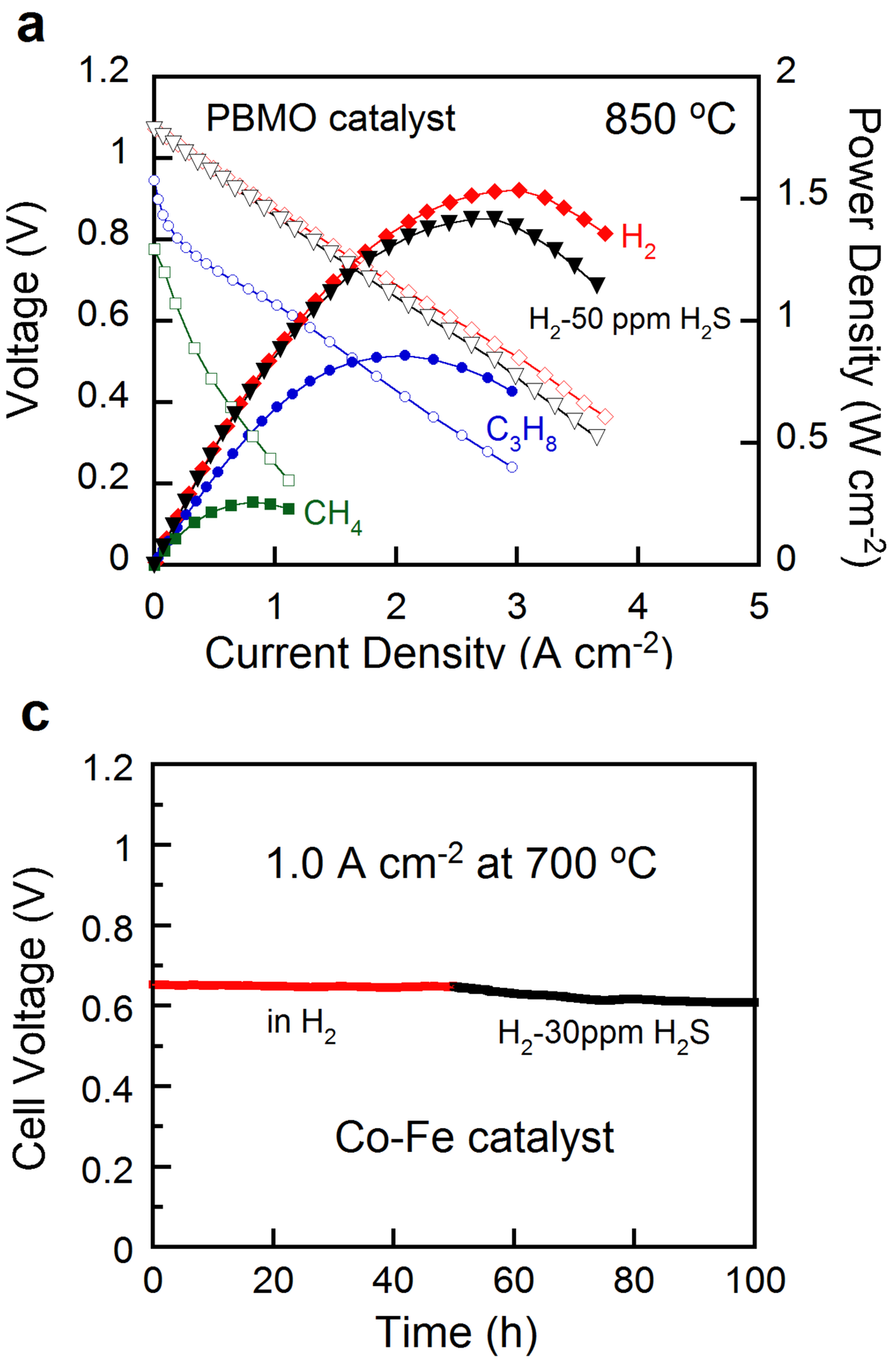
a
PBMO catalyst
850 °C
H2
H2-50 ppm H2S
C3H8
CH4
Voltage (V)
Power Density (W cm-2)
Current Density (A cm-2)

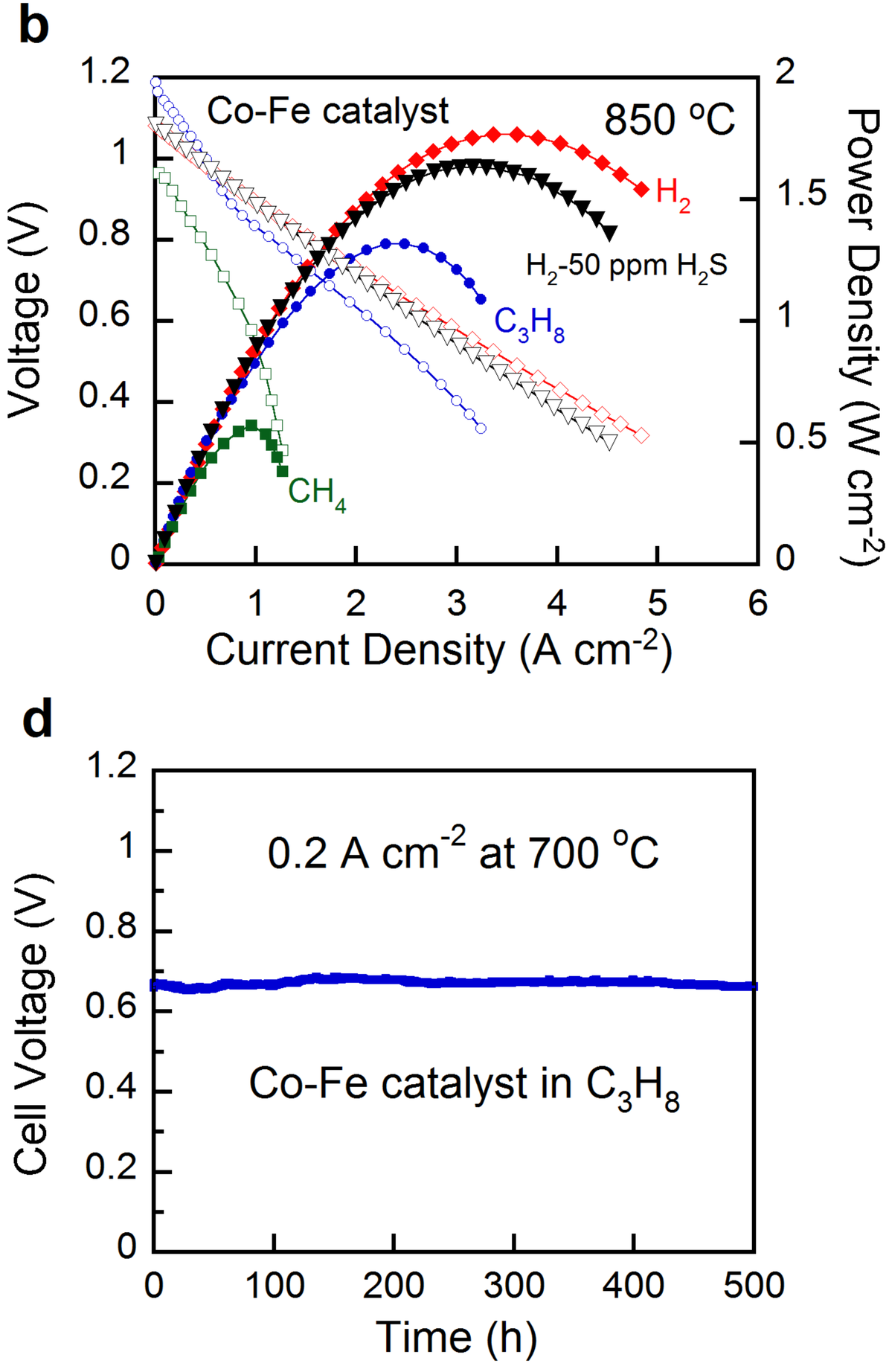
b
Co-Fe catalyst
850 °C
H2
H2-50 ppm H2S
C3H8
CH4
Voltage (V)
Power Density (W cm-2)
Current Density (A cm-2)

c
1.0 A cm-2 at 700 °C
in H2
H2-30ppm H2S
Co-Fe catalyst
Cell Voltage (V)
Time (h)

d
0.2 A cm-2 at 700 °C
Co-Fe catalyst in C3H8
Cell Voltage (V)
Time (h)